

1 **Grounding and Calving Cycle of Mertz Ice Tongue**

2 **Revealed by Shallow Mertz Bank**

3 Xianwei Wang^{1,2}, David M. Holland^{2,3}, Xiao Cheng^{1,5} and Peng Gong^{4,5}

4 1. State Key Laboratory of Remote Sensing Science, and College of Global Change and Earth System Science,
5 Beijing Normal University. Beijing 100875, China.

6 2. Center for Global Sea Level Change, New York University Abu Dhabi. Abu Dhabi, United Arab Emirates.

7 3. Courant Institute of Mathematical Sciences, New York University. New York 10012, United States of America.

8 4. Ministry of Education Key Laboratory for Earth System Modeling, and Center for Earth System Science,
9 Tsinghua University, Beijing, China 100084.

10 5. Joint Centre for Global Change Studies, Beijing, China.

11

12 *Correspondence to: wangxianwei0304@163.com*

13 **Abstract**

14 A recent study, using remote sensing, provided some evidence that a seafloor shoal
15 influenced the 2010 calving event of the Mertz Ice Tongue (MIT), by partially grounding the
16 MIT several years earlier. In this paper, we start by proposing a method to calculate Firn Air
17 Content (FAC) around Mertz from seafloor-touching icebergs. Our calculations indicate the FAC
18 around Mertz region as 4.87 ± 1.31 m. We then design an indirect method of using freeboard and
19 sea surface height data extracted from ICESat/GLAS, FAC, and relatively accurate seafloor
20 topography to detect grounding sections of the MIT between 2002 and 2008 and analyze the
21 process of grounding prior to the calving event. By synthesizing remote sensing data, we point
22 out that the grounding position was localized northeast of the Mertz ice front close to the Mertz
23 Bank. The grounding outlines of the tongue caused by the Mertz Bank are extracted as well.
24 From 2002 to 2008, the grounding area increased and the grounding became more pronounced.
25 Additionally, the ice tongue could not effectively climb over the Mertz Bank in following the
26 upstream ice flow direction and that is why MIT rotated clockwise after late 2002. Furthermore,
27 we demonstrate that the area-increasing trend of the MIT changed little after calving ($\sim 36 \text{ km}^2/\text{a}$),
28 thus allowing us to use remote sensing to estimate the elapsed time until the MIT can reground
29 on and be bent by the shoal. This period is approximately 70 years. In the calving induced by
30 iceberg collisions, our observations suggest that calving of the MIT is a cyclical process
31 controlled by the presence of the shallow Mertz Bank location and the flow rate of the tongue.
32 The calving cycle of the MIT explains the cycle of sea-surface condition change around the
33 Mertz.

34 **Keywords:** Mertz Ice Tongue, firn air content, grounding, Mertz Bank, calving cycle.

35 **1. Introduction**

36 Surface-warming induced calving or disintegration of floating ice has occurred in
37 Antarctica, such as the Larsen B ice shelf (Scambos et al., 2000, 2003; Domack et al., 2005;
38 Shepherd et al., 2003). While surface or sub-surface melting has largely been recognized to
39 contribute to floating ice loss in Antarctica (Depoorter et al., 2013), calving caused by interaction
40 with the seafloor has not been widely considered. The Mertz Ice Tongue (MIT) was reported to
41 have calved in 2010, subsequent to being rammed by a large iceberg, B-9B (Legresy et al. 2010).
42 After the calving, the areal coverage of the Mertz polynya, sea ice production and dense, shelf
43 water formation in the region changed (Kusahara et al. 2011; Tamura et al. 2012). However, the
44 iceberg collision may have only been an apparent cause of the calving as other factors had not
45 been fully considered such as seafloor interactions (Massom et al., 2015; Wang. 2014). By
46 comparing inverted ice thickness to surrounding bathymetry, and combining remote sensing,
47 Massom et al., (2015) considered that the seabed contact may have held the glacier tongue in
48 place to delay calving by ~8 years. The interaction of the MIT with the seafloor, the exact
49 grounding location of the MIT before calving and the extent of grounding are still not well-
50 known.

51 The MIT (66°S-68°S, 144°E-150°E, Fig. 1) is located in King George V Land, East
52 Antarctica, with an ice tongue extending over 140 km from its grounding line to the tongue front
53 and approximately 30 km wide at the front (Legresy et al., 2004). Much field exploration has
54 been conducted around Mertz and the increasing availability over the last decade of remote
55 sensing, hydrographic surveying, and bathymetric data allows the causes of ice tongue instability
56 to gradually come into focus. From satellite altimetry, a modest elevation change rate of 0.03 m/a
57 (Pritchard et al., 2012) and a freeboard change rate of -0.06 m/a (Wang et al., 2014) were found,

58 which implied that the combined effects of surface accumulation and basal melt were not
59 dramatic for this ice tongue. For the MIT, investigations of tidal effects, surface velocity, rift
60 propagation, and ice front propagation (Berthier et al., 2003; Frezzotti et al., 1998; Legresy et al.,
61 2004; Lescarmonier et al., 2012; Massom et al., 2010, 2015) have been conducted with an
62 objective of detecting underlying factors affecting its stability. Grounding as a potential factor
63 can affect the stability of an ice tongue by possibly holding the tongue to delay calving (Massom
64 et al. 2015). However, without highly accurate bathymetric data, it is impossible to carry out
65 such study. Fortunately, In 2010, a new and high resolution bathymetry model, with a resolution
66 of 100 m was released for the Terra Adelie and George V continental margin (Beaman et al.,
67 2011), and incidentally later used to generate the Bedmap-2 (Fretwell et al., 2013). Such
68 accurate data provides an opportunity for better exploring seafloor shoals and their impacts on
69 the instability of MIT. In this study, we focus on the grounding event of the MIT from 2002 to
70 2008. A method for grounding event detection is proposed and the grounding of the MIT before
71 calving is investigated. A calving cycle of the MIT caused by grounding on seafloor shoal, Mertz
72 Bank is discussed as well.

73 **2. Data**

74 The primary data used to investigate grounding of the MIT in this study are Geoscience
75 Laser Altimeter System (GLAS) data onboard the Ice, Cloud and land Elevation Satellite
76 (ICESat) and the seafloor bathymetry data mentioned above. In this section, ICESat/GLAS and
77 bathymetry data, as well as some preprocessing are introduced.

78 **2.1 ICESat/GLAS**

79 The ICESat is the first spaceborne laser altimetry satellite orbiting the Earth, launched by
80 National Aeronautics and Space Administration (NASA) in 2003 (Zwally et al. 2002) with

81 GLAS as the primary payload onboard. ICESat/GLAS was operated in an orbit of ~600 km and
82 had a geographical coverage from 86° S to 86° N. ICESat/GLAS usually observed in nadir
83 viewing geometry and employed laser pulses of both 532 nm and 1064 nm to measure the
84 distance from the sensor to the ground (Zwally et al. 2002). On the ground, ICESat/GLAS's
85 footprint covered an area of approximately 70 m in diameter, with adjacent footprints spaced by
86 ~170 m. The horizontal location accuracy of the footprint was about 6 m (Abshire et al. 2005).
87 The accuracy and precision of ICESat/GLAS altimetry data were 14 cm and 2 cm respectively
88 (Shuman et al. 2006). ICESat/GLAS usually made two or three campaigns a year from 2003 to
89 the end of 2009, with each campaign lasting for about one month. With billions of laser
90 footprints received by the telescope, 15 different types of data were produced for various
91 scientific applications, named as GLA01, GLA02, ... GLA15. In this study, GLA12 data
92 (elevation data for polar ice sheet) covering the Mertz from release 33 during the interval of 2003
93 to 2009 is used, the spatial distribution of which is shown in Fig. 2.

94 **2.2 Seafloor Topography**

95 Detailed bathymetry maps are fundamentally spatial data for marine science studies
96 (Beaman et al., 2003, 2011) and crucially needed in the data-sparse Antarctic coastal region
97 (Massom et al. 2015). Regionally, around Mertz, a large archive of ship track single-beam and
98 multi-beam bathymetry data from 2000 to 2008 were used to generate a high resolution Digital
99 Elevation Model (DEM), the spatial coverage of which can be found from Figs. 3(b) and 3(c).
100 The DEM product was reported as having a vertical accuracy of about 11.5 m (500 m depth) and
101 horizontal accuracy of about 70 m (500 m depth) in the poorest situation (Beaman et al. 2011).
102 As can be seen from Fig. 3(b) and Fig. 3(c), there is no bathymetry data under the MIT, which
103 may result in large uncertainty for seafloor interpolation. The oldest bathymetry data collected

104 along the margin of the MIT was at least from 2000 (Beaman et al. 2011). Thus, the boundary of
105 the MIT in 2000 is used to identify bathymetry measurement gaps, as is indicated in Fig. 6.
106 However around the Mertz ice front, for both the east and west flanks, bathymetry data does
107 exist, which provide control points for seafloor interpolation under the tongue. Since the ice front
108 has a width of ~34 km (Wang et al. 2014), the accuracy of seafloor DEM under the MIT varies
109 according to different distance to the control points. Inside of the 2000 boundary of the MIT, the
110 closer to the dash-dotted polygon (Figs. 6 and 7), the better accuracy the seafloor DEM. Outside
111 of that boundary, the quality of the seafloor DEM data is much better because of the high density
112 of single-beam or multi-beam bathymetric measurements.

113 Around Antarctica, seafloor topography data from Bedmap-2 was produced by Fretwell
114 et al. (2013) which adopted the DEM from Beaman et al. (2011). In this study, Bedmap-2
115 seafloor topography data covering Mertz is employed to detect the contact between seafloor and
116 the MIT. Because of inconsistent elevation systems for ICESat/GLAS and seafloor topography
117 data, the Earth Gravitational Model 2008 (EGM08) geoid (Pavlis et al. 2012) with respect to
118 World Geodetic System 1984 (WGS-84) ellipsoid is taken as reference. Since seafloor
119 topography from Bedmap-2 is referenced to the so-called g104c geoid, an elevation
120 transformation is required and can be implemented through Eq. (1).

$$121 \quad E_{sf} = E_{seafloor} + gl04c_{to_wgs84} - EGM2008 \quad (1)$$

122 where E_{sf} and $E_{seafloor}$ is the seafloor topography under EGM08 and g104c respectively,
123 $gl04c_{to_wgs84}$ is the value needed to convert height relative to g104c geoid to that under WGS-84,
124 and $EGM2008$ is the geoid undulation with respect to WGS-84.

125 **3. Methods**

126 **3.1 Grounding Detection Methods**

127 ICESat/GLAS data has been widely used to determine ice freeboard, or ice thickness,
128 since its launch in 2003 (Kwok et al., 2007; Wang et al., 2011, 2014; Yi et al., 2011; Zwally et
129 al., 2002, 2008). The methods we designed for grounding detection of the MIT are now
130 introduced using ICESat/GLAS data. First, assuming a floating ice tongue, based on freeboard
131 data extracted in different observation dates, the ice draft of the MIT is inverted. Next, ice
132 bottom elevation is calculated based on the inverted ice draft and the lowest sea-surface height.
133 Finally, the ice bottom is compared with seafloor bathymetry and ice grounding is detected. The
134 underlying logic for grounding detection is that if the inverted ice bottom is lower than seafloor,
135 we can draw a conclusion that the ice tongue is grounded rather than floating.

136 The method to extract a freeboard map using ICESat/GLAS from multiple campaigns
137 over the MIT was described in Wang et al. (2014). Here, we do not revisit it in detail but
138 introduce it schematically. Four steps are included in freeboard map production for each of the
139 datasets from November 14, 2002, March 8, 2004, December 27, 2006 and January 31, 2008..

140 The first step involves data preprocessing, saturation correction, data quality control, and
141 tidal correction removal. The magnitude of the ICESat/GLAS waveform can become saturated
142 because of different gain setting, or high reflected natural surface. Thus the saturated waveforms
143 with *i_satElevCorr* (i.e. an attribute from GLA12 data record) greater than or equal to 0.50 m are
144 ignored and those with *i_satElevCorr* less than 0.50 m are corrected following the procedures in
145 Wang et al. (2012, 2013). Additionally, measurements with *i_reflectUC* greater than or equal to
146 one are ignored. Furthermore, tidal correction from the TPX07.1 tide model in GLA12 data
147 record is removed to obtain estimates of the instantaneous sea surface height. Finally, elevation
148 data from ICESat/GLAS related to the WGS-84 ellipsoid and EGM 08 geoid from 2003 to 2009
149 is ready for subsequent use.

150 The second step is to derive sea-surface height according to each track and to calculate
151 freeboard for each campaign. Because of tidal variations near the MIT, surface elevations of the
152 MIT can vary as well. To derive sea-surface height from ICESat/GLAS and provide a reference
153 for freeboard calculation for different campaigns, ICESat/GLAS data over the MIT within a
154 buffer region (with 10 km as buffer radius of MIT boundary in 2007) are selected and sea-
155 surface height is determined as the lowest elevation measurement along each track (Wang et al.
156 2014). Freeboard is then calculated by subtracting the corresponding sea-surface height from
157 elevation measurements of the MIT according to different tracks in the same campaign. Thus
158 freeboard data for different campaigns from 2003 to 2009 is obtained.

159 The third step is to relocate footprints using estimated ice velocity. ICESat observed the
160 MIT almost repeatedly along different tracks in different campaigns (Fig. 2). However,
161 observation from only one campaign cannot provide good coverage of the MIT, which drives us
162 to combine all observations from 2003 to 2009 together to produce a freeboard map of MIT. Fig.
163 2 shows the spatial coverage of ICESat/GLAS from 2003 to 2009 over the Mertz, but the
164 geometric relation between tracks is not correct over the MIT because the tongue was fast
165 moving and observed in different years by the ICESat. The region observed in an earlier
166 campaign would move downstream later (Wang et al. 2014). For example, consider ICESat data
167 from track T31 on March 22, 2003 and T165 (Fig. 2) on November 1, 2003 respectively. Fig. 2
168 shows the distance between track T165 and T31 is ~ 7.5 km without accounting for ice advection
169 between observation dates. However because of the fast moving ice tongue, the distance of their
170 actual ground tracks on the surface of the MIT should be larger because T165 was located
171 upstream and observed later. Thus footprints relocation using ice velocity is critical to obtain
172 accurate geometric relations among different tracks. The ice velocity data from Rignot et al.

173 (2011) generated from InSAR data from 2006 to 2010 is used to relocate the footprints of
174 ICESat/GLAS. Thus the correct geospatial relations between observations from different
175 campaigns can be achieved on November 14, 2002, March 8, 2004, December 27, 2006, and
176 January 31, 2008, through Eqs. (2) and (3).

$$177 \quad X = x + \sum_{i=1}^n v_{xi} \Delta t + v_{xm} t_m \quad (2)$$

$$178 \quad Y = y + \sum_{i=1}^n v_{yi} \Delta t + v_{ym} t_m \quad (t_m = t_2 - t_1 - n \Delta t) \quad (3)$$

179 where x and y are locations in the X and Y directions from ICESat measurement directly;
180 X and Y are locations in the X and Y directions after relocation; v_x and v_y are the ice velocities in
181 the X and Y directions respectively; t_1 and t_2 are the start and end times; Δt is the time interval
182 and n indicates the largest integer time steps for time interval between t_1 and t_2 ; t_m is the
183 residual time; In this work, Δt is set as 10 days; v_{xi} and v_{yi} is derived from ice velocity field
184 according to different locations during relocation and may change in different time intervals.

185 The freeboard change with time should be considered as well, but this contribution is
186 neglected because freeboard comparison from crossing tracks showed a slightly decreasing trend
187 of -0.06 m/a on average (Wang et al. 2014). The spatial distribution of freeboard data over the
188 MIT corresponding to November 14, 2002, is shown in Fig. 5(a).

189 The forth step is to interpolate the freeboard map using the relocated freeboard data from
190 the third step. Kriging interpolation under spatial analysis toolbox of ArcGIS is selected in this
191 study to produce freeboard maps of the MIT because it can provide an optimal interpolation
192 estimate for a given coordinate location by considering the spatial relationships of a data set.
193 With this method, freeboard maps of the MIT are produced on November 14, 2002, March 8,
194 2004, December 27, 2006, and January 31, 2008 when the ice tongue outline can be delineated
195 from Landsat images.

196 Ice draft is calculated with Eq. (4) assuming hydrostatic equilibrium and using the lowest
197 sea-surface height which is extracted from ICESat/GLAS data from all campaigns covering this
198 region, -3.35 m under EGM 08 (WGS-84).

$$199 \quad \rho_w D = \rho_i (H_f + D - FAC) \quad (4)$$

200 where D is ice draft, i.e. vertical distance from sea surface to bottom of ice; H_f is
201 freeboard, i.e. vertical distance from sea surface to top of snow; ρ_w and ρ_i are densities of
202 ocean water and ice, respectively. In this study, ice and sea water density are taken as 915 kg/m^3
203 and 1024 kg/m^3 , respectively (Wang et al., 2014); FAC is the firm air content, the decrease in
204 thickness (in meters) that occurs when the firm column is compressed to the density of glacier ice,
205 as defined in Holland et al., (2011) and Ligtenberg et al. (2014).

206 The lowest sea surface height -3.35 m is derived by comparing all sea-surface heights
207 derived from different tracks and campaigns from 2003 to 2009. This constant stands for the
208 lowest sea surface height from results around Mertz from 2003 to 2009 and is directly from
209 ICESat/GLAS observation. For time varying sea-surface heights caused by tides, the minimum
210 sea-surface height can allow ice with a given draft to ground to the seafloor. Then, ice bottom
211 elevation is calculated by considering the ice draft and the lowest sea-surface height. To compare
212 the ice bottom with the seafloor, an elevation difference of both is calculated. In this way, a
213 negative value indicates that ice bottom is lower than the seafloor, which corresponds to
214 grounding.

215 The calculation of firm air content around Mertz is introduced in Section 3.2. In this work,
216 we define the elevation of the underside (bottom) of the tongue as E_{ice_bottom} and is calculated
217 by Eq. (5).

$$218 \quad E_{ice_bottom} = E_{sea_level} - D \quad (5)$$

219 where E_{ice_bottom} corresponds to elevation of the ice bottom. E_{sea_level} is the lowest sea-surface
220 height among extracted sea-surface height from different tracks and different campaigns, which
221 is -3.35 m.

222 Similarly, the elevation difference of ice tongue bottom and seafloor is defined as E_{dif} ,
223 which can be calculated by Eq. (6).

$$224 \quad E_{dif} = E_{ice_bottom} - E_{sf} \quad (6)$$

225 where E_{sf} is the seafloor elevation as defined in Eq. (1).

226 **3.2. Firn Air Content Estimation Method**

227 The Antarctic ice sheet is covered by a dry, thick firn layer which represents an
228 intermediate stage between fresh snow and glacial ice, having varying density from Antarctic
229 inland to the coast (van den Broeke, 2008). The density and depth of the Antarctic firn layer has
230 been modeled (e.g., van den Broeke, 2008) using a combination of regional climate model output
231 and a steady-state firn compaction model. However, for ice thickness inversion, Firn Air Content
232 (FAC) is usually used to make the calculation convenient (Rignot and Jacobs, 2002). FAC is
233 defined as the decrease in thickness (in meters) that occurs when the firn column is compressed
234 to the density of glacier ice (Holland et al., 2011). Time-dependent FAC has also been modeled
235 by considering the physical process of the firn layer (e.g., Ligtenberg et al. 2014). For the MIT,
236 there are some in-situ measurements of snow thickness available from Massom et al. (2010) who
237 used a snow layer depth of 1 m to derive the thickness of surrounding multi-year, fast sea ice.
238 However on the surface of the MIT, no in-situ measurements of density or depth of firn layer is
239 available.

240 Because of different density and thickness of the firn layer on top of an ice tongue, it is
241 challenging to simulate the density profile of the MIT without in-situ measurements as control

242 points. In this study, we use FAC extracted from adjacent seafloor-touching icebergs to
243 investigate the grounding of the MIT rather than FAC from modeling. MIT may be composed of
244 pure ice, water, air, firn or snow that will influence the density of the ice tongue. However, if
245 assuming a pure ice density only to calculate ice mass, the thickness of MIT must be corrected
246 by FAC. FAC correction to ice thickness can be inferred from surrounding icebergs calving from
247 MIT using Eq. (4) when knowing ice draft and freeboard assuming hydrostatic equilibrium. Thus
248 it is critical to target and use icebergs fulfilling these requirements to solve Eq. (4), such as
249 slightly grounded icebergs above already known seafloor with observed freeboard. From Smith
250 (2011), icebergs can be divided into three categories based on bathymetry and seasonal pack ice
251 distributions: grounded, constrained, and free-drifting icebergs. Without occurrence of pack ice,
252 an iceberg can be free-drifting or grounded. Free-drifting icebergs can move several tens of
253 kilometers per day, such as iceberg A-52 (Smith et al. 2007). Grounded icebergs can be heavily
254 or lightly anchored. Heavily grounded icebergs have firm contact with the seafloor and can be
255 stationary for a long time, such as iceberg B-9B (Massom. 2003). However, slightly grounded
256 icebergs may have little contact with the seafloor and can possibly move slowly under the
257 influence of ocean tide, ocean currents, or winds, but much slower than free-drifting icebergs.
258 The relation of grounded iceberg to ice drifting velocity is not well-known. However, from
259 slowly drifting or nearly stationary icebergs in open water, we can determine if an iceberg is
260 slightly grounded.

261 Because of the heavily grounded iceberg B-9B to the east of the MIT blocking the
262 drifting of pack ice or icebergs from the east, icebergs located between B-9B and the MIT are
263 most likely generated from the Mertz or Ninnis glaciers. Some icebergs may be slightly
264 grounded as can be detected from remote sensing. We calculate the FAC from these slightly

265 grounded icebergs and later apply it to grounding event detection of the MIT. Around the MIT,
266 the locations of three icebergs ('A', 'B' and 'C') were identified using MODIS and Landsat
267 images in austral summer, 2006 and 2008 and shown in Fig. 4. Fortunately, ICESat/GLAS
268 observed these icebergs on February 23, 2006 (54th day of 2006) and February 18, 2008 (49th
269 day of 2008). This allows us to analyze the behavior of the icebergs three-dimensionally. From
270 Fig. 4a, icebergs 'A', 'B' and 'C' changed position little in about two months (from 28 to 85 day
271 of 2006). Thus we can consider these icebergs slightly grounded. For these slightly grounded
272 icebergs, hydrostatic equilibrium should still apply, so the ice draft inverted from freeboard
273 measurement assuming hydrostatic equilibrium should be equal to water depth. Based on this
274 analysis, we can take water depth as draft to calculate the FAC.

275 Because only 'A' and 'C' were observed by track T1289 of the ICESat/GLAS in 2006,
276 freeboard and water depth from bathymetry for both are used to calculate the FAC (Figs. 3b, 3c,
277 4, and Table 1). However, the icebergs were not stationary, which indicates only some parts were
278 slightly grounded. In this study, only the top two largest freeboard measurements of icebergs 'A'
279 and 'C' from T1289 in 2006 are employed to calculate the FAC with Eq. (7) with a least-squares
280 method under hydrostatic equilibrium.

$$281 \quad FAC = H_{f_k} + D_k - \frac{\rho_w}{\rho_i} D_k + \varepsilon_k \quad (7)$$

282 where k is used to identify different icebergs 'A' or 'C', H_f is the top two largest freeboard
283 measurement of each iceberg, D is ice draft which is the same as sea water depth and is taken
284 from seafloor bathymetry directly, ε is a residual for FAC.

285 Table 1 shows the freeboard and seafloor bathymetry under the icebergs in 2006 for FAC
286 calculation and grounding detection of icebergs in 2008 (detailed freeboard values for these
287 icebergs can be seen from S-Fig. 1). With freeboard and seafloor measurements from icebergs 'A'

288 and 'C' in 2006 (Table 1), FAC is calculated as about 4.87 ± 1.31 m. Two icebergs 'A' and 'B'
289 were observed by the same track T1289 of the ICESat/GLAS on February 18, 2008 and thus are
290 used to evaluate the grounding detection by using this FAC. From iceberg trajectories observed
291 by remote sensing (Fig. 4b), we know, iceberg 'A' drifted away from its original position. Thus
292 it was not grounded. However, iceberg 'B' kept rotating in this period without drifting away,
293 from which we can consider it slightly grounded. Such grounding status determined from remote
294 sensing can also be detected with our method since the elevation difference of ice bottom and
295 seafloor from Table 1 does clearly indicate a slightly grounded iceberg 'B' and a floating iceberg
296 'A'. Thus, our FAC estimation works well around Mertz.

297 FAC varies across the Antarctica ice sheet, usually decreasing from the interior to the
298 coast. In this section, FAC over Mertz region is derived as 4.87 ± 1.31 m. However other time
299 dependent modeling results from the Mertz region were close to 5-10 meters (Ligtenberg et al.
300 2014). Since there are no in-situ measurements available for verification, further comparison
301 work needs to be conducted. However, this FAC value is derived according to our best
302 knowledge over Mertz and is affected by iceberg status and the maximum freeboard used. Our
303 method is not perfect and there are some shortcomings which should be paid attention to.

304 First, for FAC calculation, icebergs just touching the seafloor should be used in which
305 case the FAC calculated assuming hydrostatic equilibrium is the same as the actual value.
306 However, it is difficult to ascertain whether an iceberg is just touching the seafloor from remote
307 sensing images. The near stationary or slowly rotating iceberg detected with remote sensing may
308 be grounded more severely than those just touching the seafloor, which may result in a calculated
309 FAC theoretically larger than the actual value. Thus, using this FAC result to detect grounding

310 can potentially lead to smaller grounding results. However, once an iceberg or ice tongue is
311 detected as grounded using this FAC content, the result is more convincing.

312 Second, limited observation from ICESat/GLAS may not catch the same and the thickest
313 section of an iceberg. Because ICESat/GLAS observed only several times a year on repeat tracks
314 and icebergs were rotating slowly, the elevation profile in 2006 and 2008 along the same track
315 T1289 may not come from the same ground surface. S-Fig. 1 shows the freeboard of icebergs
316 ‘A’, ‘B’ and ‘C’ derived from ICESat/GLAS from 2006 and 2008. By comparing freeboard of
317 iceberg ‘A’ in 2006 (S-Fig. 1a), and 2008 (S-Fig. 1c), we can find that the maximum freeboard
318 was larger and the freeboard profile was longer in 2006. Comparatively, the smaller freeboard in
319 2008 may be caused by basal melting or observing different portion of iceberg ‘A’. Since the
320 larger freeboard measured in 2006 indicates a high possibility of capturing the thickest portion,
321 the freeboard measurement in 2006 is used to invert the FAC. Additionally, iceberg ‘A’ and ‘C’
322 did show the similar maximum freeboard (Table 1), which is another important reason to select
323 the measurements in 2006 to invert.

324 **4. Accuracy of Grounding Detection**

325 The accuracy of E_{dif} is critical to grounding detection of the MIT. From Eq. (1) to (6),
326 we find different components of the error sources, such as from sea surface height determination,
327 ice draft, seafloor bathymetry, and elevation transformation. Meanwhile, uncertainty of ice draft
328 is primarily determined by that of freeboard and FAC . Furthermore, the uncertainty of freeboard
329 is influenced by footprint relocation and freeboard changing rates. Considering all mentioned
330 above, the error source of elevation difference E_{dif} can be synthesized by Eq. (8):

$$331 \Delta E_{dif} = \Delta E_{sl} + a(\Delta H_f + \Delta E_{re} + \Delta E_{fbc} + \Delta FAC + \Delta E_{krig}) + \Delta E_{sf} + \Delta E_{trans} \quad (8)$$

332 where $a = \frac{\rho_i}{\rho_w - \rho_i}$; Δ stands for error of each variable; ΔE_{dif} stands for error of final elevation
 333 difference of ice bottom and seafloor; ΔE_{sl} , ΔH_f , ΔE_{re} , ΔE_{fb_c} , ΔFAC , ΔE_{sf} , ΔE_{krig} , and
 334 ΔE_{trans} stand for errors caused by sea surface height extraction, freeboard extraction, freeboard
 335 relocation, freeboard changing rates, FAC calculation, seafloor bathymetry, kriging interpolation
 336 and elevation system transformation, respectively.

337 Usually, the influence of elevation system transformation on final elevation difference
 338 can be neglected. Based on the error propagation law, the uncertainty of elevation difference E_{dif}
 339 can be described by Eq. (9):

$$340 \quad \varepsilon E_{dif} = \sqrt{(\varepsilon E_{sl})^2 + a^2 [(\varepsilon H_f)^2 + (\varepsilon E_{re})^2 + (\varepsilon E_{fb_c})^2 + (\varepsilon FAC)^2 + (\varepsilon E_{krig})^2] + (\varepsilon E_{sf})^2} \quad (9)$$

341 where ε indicates the uncertainty of each parameter.

342 **4.1 Uncertainty of kriging interpolation**

343 Fig. 5a shows the spatial distribution of freeboard data over the MIT used for detecting
 344 grounding on November 14, 2002. The spatial difference of ICESat/GLAS between Fig. 2 and
 345 Fig. 5 is caused by footprint relocation, after which the spatial geometry between different tracks
 346 is reasonably correct. In the lower right of the Mertz ice front (Fig. 5a), the crossing track
 347 distance between track T1289 and T165 is about 7 km. In these data gaps, freeboard data used
 348 for grounding detection is interpolated using kriging. Thus, knowing the uncertainty of kriging
 349 interpolation is critical to final grounding detection.

350 To investigate interpolation uncertainty of the kriging method, freeboard measurements
 351 should be compared with interpolated freeboard estimates. Thus, a testing region with freeboard
 352 measurements is selected, indicated by a dashed blue square in Fig. 5a, about 7 km×7 km. A

353 freeboard map is first interpolated with gray dots only (Fig. 5a) using kriging. Then, the
354 freeboard measurements (284 of green dots in Fig. 5a) are compared with interpolation in the
355 square. The spatial distribution and the histogram of freeboard difference derived by subtracting
356 krigged freeboard from freeboard derived from ICESat/GLAS are shown in Fig. 5b.

357 In this square, the freeboard measurement varies from 31.6 m to 40.0 m with 36.6 m in
358 average. However, the interpolated freeboard varies from 32.9 m to 39.6 m with 35.9 m in
359 average. From the freeboard difference results (Fig. 5b), we find that the interpolated freeboards
360 show similar results compared with freeboard derived from ICESat/GLAS. The interpolated
361 freeboard has an accuracy of -0.7 ± 1.8 m. The interpolated freeboard using kriging can reflect
362 the actual freeboard well.

363 **4.2 Grounding Detection Robustness**

364 Since sea surface height is extracted from ICESat/GLAS data track by track, we use
365 ± 0.15 m (Zwally et al. 2002) as the uncertainty of elevation data (εE_{st}). Also from Wang et al.
366 (2014), we can see the uncertainty of freeboard extraction (εH_f) is ± 0.50 m. From Rignot et al.
367 (2011), the error of ice velocity ranged from 5 m/a to 17 m/a. Assuming that ice velocity varied
368 by 17 m/a (an upper threshold), the relocation error horizontally could reach ± 54 m in an average
369 of three years. Wang et al. (2014) extracted the average slope of the MIT along ice flow direction
370 as 0.00024. However, because of large crevasses on the surface, we use 50 times of this value as
371 a conservative estimate of the average slope. In this way, we can estimate εE_{re} as ± 0.65 m when
372 considering a three-year period. The annual rate of freeboard change from 2003 to 2009 is -0.06
373 m/a (Wang et al. 2014). Therefore, we consider the freeboard stable over this period. However
374 when combining data from different time periods, εE_{fb_c} is estimated as about ± 0.18 m if
375 considering three-year's time difference. From Beaman et al. (2011), considering elevation

376 uncertainty at the worst situation when water depth is 500 m, εE_{g104c} is ± 11.5 m. For kriging
377 interpolation, from analysis in Section 4.1, 1.8 m is taken as the uncertainty. Using all these
378 errors above, we calculate the final uncertainty of elevation difference as ± 23 m.

379 From the calculations above, we can say that E_{dif} less than -23 m corresponds to a very
380 robust grounding event. However, if E_{dif} is greater than 23 m, we cannot confirm grounding.
381 E_{dif} in the interval of -23 m to 23 m corresponds to slightly grounding or floating. We can also
382 determine different contributions of each separate factor to the overall accuracy. Seafloor
383 bathymetry contributes the largest part and is the dominant factor affecting the accuracy of
384 grounding detection.

385 **5. Grounding Detection Results**

386 The spatial distribution of elevation difference E_{dif} and outlines of the MIT from 2002 to
387 2008 are shown in Fig. 6. A buffer region with radius of 2 km (region between black and grey
388 lines in Fig. 6) is introduced to investigate grounding potential of the MIT, if it approached there.
389 The elevation difference less than 46 m (twice of elevation difference uncertainty εE_{dif}) both
390 inside and outside of the outline is extracted and the corresponding statistics are shown in Table
391 2. Since the uncertainty to determine a grounding event is about ± 23 m, if some grid points of the
392 MIT have elevation difference E_{dif} less than -23 m, we can conclude that this section of the
393 tongue is strongly grounded. The smaller the E_{dif} , the more robust the grounding.

394 As illustrated from Table 2, the minimum E_{dif} inside of the MIT in 2002 was 11.9 m and
395 the minimum E_{dif} inside of the MIT were all less than -23 m after 2002. The minimum of the
396 E_{dif} in the buffer region were all less than -23 m from 2002 to 2008. From this point of view, we
397 conclude that the ice tongue had grounded on the shallow Mertz Bank at least since November
398 14, 2002. This result coincides with findings from Massom et al. (2015) who considered that the

399 northwestern extremity of the MIT started to contact with the seafloor shoal in late 2002 to early
400 2003. Also, it would be difficult for the MIT to approach the buffer region (indicated with yellow
401 to red colors in Fig. 6) as the surrounding Mertz Bank gets shallower and steeper, suggesting
402 substantive grounding potentials. Inside of the MIT, the minimum of elevation difference was
403 just 11.9 m on November 14, 2002, which indicates slightly grounding. However on March 8,
404 2004, December 27, 2006, and January 31, 2008, the minimum of elevation difference reached -
405 46.0 m, -52.3 m and -34.8m respectively, which means strongly grounding occurred in some
406 regions. From 2002 to 2008, more regions under the MIT had E_{dif} less than 46 m, the area of
407 which increased from 8 km² to 17 km². Additionally, the mean of E_{dif} under of the tongue for
408 those having E_{dif} less than 46 m gradually decreased from 28.8 m to 12.3m, according to which
409 we can conclude that the ice front became more firmly grounded as time passed on. Additionally,
410 since the grounding area increased from 8 km² to 17 km² (Table 2) and the mean of E_{dif}
411 decreased from 2002 to 2008, we can say that over the period from 2002 to 2008, the grounding
412 of the northwest flank of the MIT became more widespread.

413 Based on the calculated elevation difference, the grounding outlines of the MIT are
414 delineated for November 14, 2002, March 8, 2004, December 27, 2006 and January 31, 2008,
415 (Fig. 7). For the grounding part of the outline in different years, starting and ending location and
416 perimeter are also extracted, from which we can conclude that the length of the grounding
417 outline of the Mertz Bank was only limited to a few kilometers (Table 3). We find that the lower
418 right (northwest) of the MIT was always grounded and that grounding did not occur in other
419 regions (Fig. 6). The shallowest seafloor elevation the ice front touched was ~ -290 m in
420 November 2002. In 2004, 2006, and 2008, the lower right (northwest) of the MIT even
421 approached the contour of -220 m.

422 6. Discussion

423 6.1 Area Changing Rate and ~70-year Calving Cycle of MIT

424 Using Landsat TM/ETM+ images from 1989 to 2013, outlines of the MIT are extracted
425 manually. Assuming a fixed grounding line position, the area of the MIT over this period is
426 calculated. Using these data, from 1989 to 2007, an increasing area rate of the MIT is shown
427 (from 5453 km² to 6126 km²) in Fig. 8. However, the area of the MIT was almost constant from
428 2007 to 2010, before calving. The largest area of the MIT was 6113 km² closest to the calving
429 event in 2010. After the calving, the area decreased to 3617 km² in November 2010.

430 The rate of area change for the MIT from 1989 to 2007 is also obtained using a least-
431 squares method, corresponding to 35.3 km²/a. However, after the calving a slight higher area-
432 increasing trend of 36.9 km²/a, is found (Fig. 8). On average, the area-increasing rate of the MIT
433 was 36 km²/a.

434 The surface behavior such as ice flow direction changes and middle rift changes caused
435 by grounding was analyzed by Massom et al. (2015). In the history of the MIT, one or two large
436 calving events were suspected to have happened between 1912 and 1956 (Frezzotti et al., 1998).
437 Based on the interactions between the MIT and Mertz Bank suggested by our observations and
438 described below, it is likely that only one large calving event occurred between 1912 and 1956.
439 When the ice tongue touched the bank, the bank started to affect the stability of the tongue by
440 bending the ice tongue clockwise to the east, as can be seen from velocity changes from Massom
441 et al. (2015). With continuous advection of ice and flux input from upstream, a large rift from the
442 west flank of the tongue would ultimately have to occur and could potentially calve the tongue.
443 A sudden length shortening of the tongue can be caused by such ice tongue calving as indeed had
444 happened in February, 2010. We also consider that even without a sudden collision of iceberg B-

445 9B in 2010, the ice tongue would eventually calve because of existence of the shallow Mertz
446 Bank.

447 If we take 6127 km^2 as the maximum area of the MIT, assuming a constant area-changing
448 rate of about $36.9 \text{ km}^2/\text{a}$ after 2010, it will take about 68 years to calve again. When assuming an
449 area changing rate of about $35.3 \text{ km}^2/\text{a}$ as before 2010, it will take a little longer, about 71 years.
450 Therefore, without considering accidental event such as collision with other large icebergs, the
451 MIT is predicted to calve again in ~ 70 years. Because of the continuous advection of ice from
452 upstream and the fixed location of the shallow Mertz Bank, the calving is likely repeatable and a
453 cycle therefore exists.

454 After the MIT calved in February, 2010, Mertz polynya size, sea-ice production, sea-ice
455 coverage and high-salinity shelf water formation changed. A sea-ice production decrease of
456 about 14-20% was found by Tamura et al. (2012) using satellite data and high-salinity shelf
457 water export was reported to reduce up to 23% using a state-of-the-art ice-ocean model
458 (Kusahara et al. 2010). Recently, Campagne et al. (2015) pointed out a ~ 70 -year cycle of surface
459 ocean condition and high-salinity shelf water production around Mertz through analyzing
460 reconstructed sea ice and ocean data over the last 250 years. They also mentioned that this cycle
461 was closely related to presence and activity of the Mertz polynya. However, the reason for this
462 cycle was not fully understood.

463 From these findings addressed above and MIT calving cycle we found, our explanation is
464 that the calving cycle of the MIT leads to the ~ 70 -year cycle of surface ocean condition and
465 high-salinity shelf water production around Mertz. Different length of the MIT can prevent sea
466 ice drifting from east side differently. A long MIT contributes to maintain a large polynya
467 because more sea ice formed on the east side could not drift to the west side. With the effect of

468 katabatic wind, sea ice produced from the west side is blown seaward which maintains polynya
469 size and stable sea ice production. Calving decreases the length of the MIT suddenly. Then, a
470 short ice tongue reduces the size of Mertz Polynya formed by Antarctic katabatic winds,
471 resulting in lower sea-ice production and further lessens high-salinity shelf water production.
472 Therefore, the cycle of ocean conditions around Mertz found by Campagne et al. (2015) is likely
473 dominated by the calving of the MIT. Additionally, the 70 year cycles of MIT calving coincides
474 with surface ocean condition change around Mertz well which makes the explanation much more
475 compelling.

476 **6.2 Seafloor DEM**

477 High accuracy seafloor elevation is critical to the final success of grounding detection.
478 Since Beaman et al. (2011) provided the most accurate seafloor DEM over Mertz according to
479 our best knowledge, seafloor DEM inside of dash-dotted polygon (Fig. 7) is kept and the
480 grounding detection is conducted there (Fig. 6) as well. Additionally, the ice tongue never
481 stopped flowing further into the ocean, where the bathymetry measurements density is good.
482 From results shown in Fig. 6 all grounding sections of MIT boundary are located outside of the
483 2000 boundary. Thus the analysis of grounding detection near ice front in 2002, 2004, 2006, and
484 2008 is convincing. Inside of the 2000 boundary, most of the grounding detection results are
485 above 100 m, indicating a floating status of the corresponding ice. Only abnormal seafloor
486 features higher than this seafloor DEM by about 100 m can result in wide grounding inside.
487 Actually, no matter whether the MIT inside of the 2000 boundary was grounded or not, gradual
488 grounding on the shallow Mertz Bank of the MIT since late 2002 is a fact, which is direct
489 evidence for us to infer the primary cause of the instability of the MIT.

490 **6.3 Influence of Mertz Bank on MIT**

491 Fig. 7 shows the extension line of west flank in November, 2002, from which we can see
492 that if the MIT advected along the former direction, the ice flow would be seriously blocked
493 when approaching the Mertz Bank. The shallowest region of the Mertz Bank has an elevation of
494 about -140 m and the MIT would have to climb the 140 m obstacle to cross it. The shallow Mertz
495 Bank would have caused strongly grounding during the climbing. This special feature of seafloor
496 shoal facing the MIT can further explain why the ice velocity differed along the east and west
497 flanks of the MIT before calving and why the ice tongue was deflected clockwise to the east, as
498 pointed out by Massom et al. (2015). However, because of sparsely-distributed bathymetry data
499 (point measurements) in Mertz region used in Massom et al. (2015), this effect could not be
500 easily seen. Here, from our grounding detection results and surrounding high-accuracy
501 bathymetry data, this effect is more clearly observed.

502 **7. Conclusion**

503 In this study, a method of FAC calculation from seafloor-touching icebergs around Mertz
504 region is presented as an important element of understanding MIT grounding. The FAC around
505 the Mertz is about 4.87 ± 1.31 m. This FAC is used to calculate ice draft based on sea surface
506 height and freeboard extracted from ICESat/GLAS and is verified working well. A method to
507 extract grounding sections of the MIT is described based on comparing inverted ice draft
508 assuming hydrostatic equilibrium with seafloor bathymetry. The final grounding results explain
509 the surface behavior of the MIT. Previous work by Massom et al. (2015) has also provided some
510 evidence for seafloor interaction, in showing that the MIT front had an approximate 280 m draft
511 with the nearby seafloor as shallow as 285 m, suggesting the possibility of grounding. In our
512 work, we have provided ample detailed bathymetry and ice draft calculations. Specifically, ice
513 bottom elevation is inverted using ICESat/GLAS data and compared with seafloor bathymetry

514 during 2002, 2004, 2006, and 2008. From those calculations we show conclusively that the MIT
515 was indeed grounded along a specific portion of its northwest flank over a limited region. We
516 also point out that even without collision by iceberg B-9B in early 2010 the ice tongue would
517 eventually have calved because of ice advection from the upstream and glacier flow being
518 increasingly opposed by a reaction force from the seafloor shoal of the Mertz Bank.

519 From remote sensing images we are able to quantify the rate of increase of area of the
520 MIT before and after the 2010 calving. While the area-increasing trend of the MIT after calving
521 is slightly larger than before, we use the averaged rate to estimate a timescale required for the
522 MIT to re-advance to the area of the shoaling bathymetry from its retreated, calved position. Our
523 estimate is ~70-years, which is remarkably consistent with Campagne et al. (2015) who found a
524 similar period of sea surface changes using seafloor sediment data. A novel point we bring out in
525 our study is that it is the shoaling of the seafloor combined with the rate of advance of the MIT
526 that leads to the 70-year repeat cycle. Also the calving cycle of the MIT explains the observed
527 cycle of sea surface conditions change well, which indicates the calving of the MIT is the
528 dominant factor for sea-surface condition change. Understanding the mechanism underlying the
529 periodicity of MIT calving is important as the presence or absence of the MIT has a profound
530 impact on sea ice and hence of bottom water formation in the local region.

531 **Acknowledgements**

532 This research was supported by Fundamental Research Fund for the Central University,
533 the Center for Global Sea Level Change (CSLC) of NYU Abu Dhabi (Grant: G1204), the Open
534 Fund of State Key Laboratory of Remote Sensing Science (Grant: OFSLRSS201414), and the
535 China Postdoctoral Science Foundation (Grant: 2012M520185, 2013T60077). We are grateful to
536 the Chinese Arctic and Antarctic Administration, the European Space Agency for free data

537 supply under project C1F.18243, the National Snow and Ice Data Center (NSIDC) for the
538 availability of the ICESat/GLAS data (<http://nsidc.org/data/order/icesat-glas-subsetter>) and
539 MODIS image archive over the Mertz glacier ([http://nsidc.org/cgi-](http://nsidc.org/cgi-bin/modis_iceshelf_archive.pl)
540 [bin/modis_iceshelf_archive.pl](http://nsidc.org/cgi-bin/modis_iceshelf_archive.pl)), British Antarctica Survey for providing Bedmap-2 seafloor
541 topography data (<https://secure.antarctica.ac.uk/data/bedmap2/>), the National Geospatial-
542 Intelligence Agency for publicly released EGM2008 GIS data ([http://earth-](http://earth-info.nga.mil/GandG/wgs84/gravitymod/egm2008/egm08_gis.html)
543 [info.nga.mil/GandG/wgs84/gravitymod/egm2008/egm08_gis.html](http://earth-info.nga.mil/GandG/wgs84/gravitymod/egm2008/egm08_gis.html)), and the USGS for Landsat
544 data (<http://glovis.usgs.gov/>). Fruitful discussions with M. Depoorter, P. Morin, T. Scambos and
545 R. Warner, and constructive suggestions from Editor Andreas Vieli and two anonymous
546 reviewers are acknowledged.

547 **References**

- 548 1. Abshire, J. B., Sun, X., Riris, H., Sirota, J. M., McGarry, J. F., Palm, S., ... & Liiva, P.
549 (2005). Geoscience laser altimeter system (GLAS) on the ICESat mission: on - orbit
550 measurement performance. *Geophysical Research Letters*, 32(21).
- 551 2. Beaman, R. J., & Harris, P. T. (2003). Seafloor morphology and acoustic facies of the
552 George V Land shelf. *Deep Sea Research Part II: Topical Studies in Oceanography*,
553 50(8), 1343-1355.
- 554 3. Beaman, R. J., O'Brien, P. E., Post, A. L., & De Santis, L. (2011). A new high-resolution
555 bathymetry model for the Terre Adélie and George V continental margin, East Antarctica.
556 *Antarctic Science*, 23(01), 95-103.
- 557 4. Berthier, E., Raup, B., & Scambos, T. (2003). New velocity map and mass-balance
558 estimate of Mertz Glacier, East Antarctica, derived from Landsat sequential imagery.
559 *Journal of Glaciology*, 49(167), 503-511.

- 560 5. Campagne, P., Crosta, X., Houssais, M. N., Swingedouw, D., Schmidt, S., Martin, A., ...
561 & Massé G. (2015). Glacial ice and atmospheric forcing on the Mertz Glacier Polynya
562 over the past 250 years. *Nature Communications*, 6.
- 563 6. Depoorter, M. A., Bamber, J. L., Griggs, J. A., Lenaerts, J. T. M., Ligtenberg, S. R. M.,
564 van den Broeke, M. R., & Moholdt, G. (2013). Calving fluxes and basal melt rates of
565 Antarctic ice shelves. *Nature*, 502(7469), 89-92.
- 566 7. Domack, E., Duran, D., Leventer, A., Ishman, S., Doane, S., McCallum, S., ... & Prentice,
567 M. (2005). Stability of the Larsen B ice shelf on the Antarctic Peninsula during the
568 Holocene epoch. *Nature*, 436(7051), 681-685.
- 569 8. Fretwell, P., Pritchard, H. D., Vaughan, D. G., Bamber, J. L., Barrand, N. E., Bell, R., ...
570 & Fujita, S. (2013). Bedmap2: improved ice bed, surface and thickness datasets for
571 Antarctica. *Cryosphere*, 7(1).
- 572 9. Frezzotti, M., Cimbelli, A., & Ferrigno, J. G. (1998). Ice-front change and iceberg
573 behaviour along Oates and George V Coasts, Antarctica, 1912-96. *Annals of Glaciology*,
574 27, 643-650.
- 575 10. Holland, P. R., Corr, H. F., Pritchard, H. D., Vaughan, D. G., Arthern, R. J., Jenkins, A.,
576 & Tedesco, M. (2011). The air content of Larsen ice shelf. *Geophysical Research Letters*,
577 38(10).
- 578 11. Kusahara, K., Hasumi, H. & Williams, G. D. (2011), Impact of the Mertz Glacier Tongue
579 calving on dense water formation and export. *Nature communications*, 2, 159.
- 580 12. Kwok, R. Cunningham, G. F., Zwally, H. J., & Yi, D. (2007). Ice, Cloud, and land
581 Elevation Satellite (ICESat) over Arctic sea ice: retrieval of freeboard. *Journal of*
582 *Geophysical Research*, 112, C12013, doi:10.1029/2006JC003978.

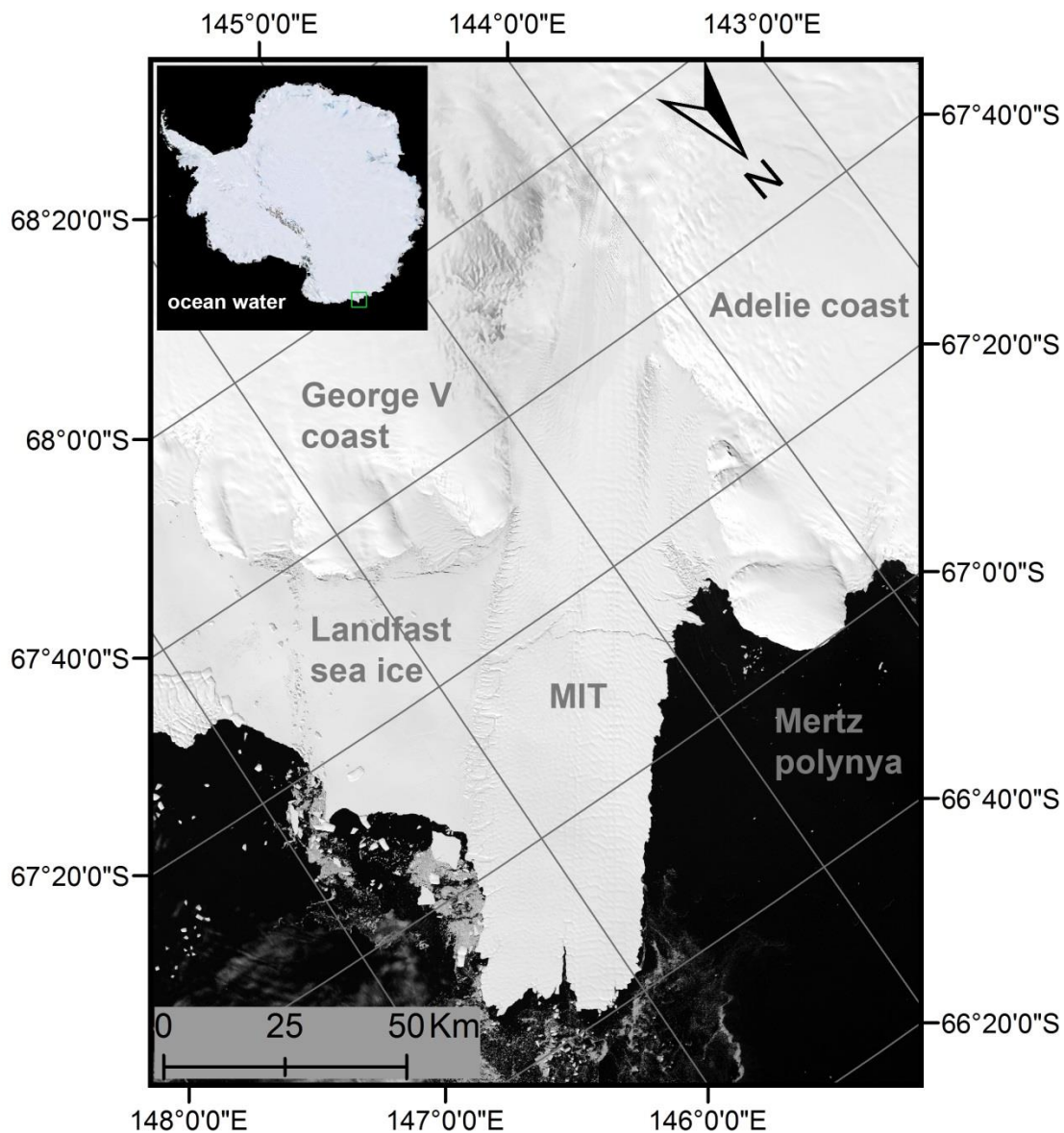
- 583 13. Legresy, B., Wendt, A., Tabacco, I. E., Remy, F., & Dietrich, R. (2004). Influence of
584 tides and tidal current on Mertz Glacier, Antarctica. *Journal of Glaciology*, 50(170), 427-
585 435.
- 586 14. Legresy, B., N. Young, L. Lescarmonier, R. Coleman, R. Massom, B. Giles, A. Fraser, R.
587 Warener, B. Galton-Fenzi, L. Testut, M. Houssais and G. Masse (2010), CRAC!!! in the
588 Mertz Glacier, Antarctica.
589 [http://www.antarctica.gov.au/__data/assets/pdf_file/0004/22549/ml_402353967939815_](http://www.antarctica.gov.au/__data/assets/pdf_file/0004/22549/ml_402353967939815_mertz_final_100226.pdf)
590 [mertz_final_100226.pdf](http://www.antarctica.gov.au/__data/assets/pdf_file/0004/22549/ml_402353967939815_mertz_final_100226.pdf)
- 591 15. Lescarmonier, L., Legrésy, B., Coleman, R., Perosanz, F., Mayet, C., & Testut, L. (2012).
592 Vibrations of Mertz glacier ice tongue, East Antarctica. *Journal of Glaciology*, 58(210),
593 665-676.
- 594 16. Ligtenberg, S., Kuipers Munneke, P., & Van Den Broeke, M. R. (2014). Present and
595 future variations in Antarctic firn air content. *The Cryosphere*, 8(5), 1711-1723.
- 596 17. Massom, R. A. (2003). Recent iceberg calving events in the Ninnis Glacier region, East
597 Antarctica. *Antarctic Science*, 15(02), 303-313.
- 598 18. Massom, R. A., Giles, A. B., Fricker, H. A., Warner, R. C., Legrésy, B., Hyland, G.,
599 Young, N., & Fraser, A. D. (2010). Examining the interaction between multi-year
600 landfast sea ice and the Mertz Glacier Tongue, East Antarctica: Another factor in ice
601 sheet stability? *Journal of Geophysical Research*, 115, C12027,
602 doi:10.1029/2009JC006083.
- 603 19. Massom, R. A., Giles, A. B., Warner, R. C., Fricker, H. A., Legrésy, B., Hyland, G., ... &
604 Young, N. (2015). External influences on the Mertz Glacier Tongue (East Antarctica) in

- 605 the decade leading up to its calving in 2010. *Journal of Geophysical Research: Earth*
606 *Surface*, 120(3), 490-506.
- 607 20. Pavlis, N. K., Holmes S. A., Kenyon, S. C., & Factor, J. K. (2012). The development and
608 evaluation of the Earth Gravitational Model 2008 (EGM2008), *Journal of Geophysical*
609 *Research*. 117, B04406, doi:10.1029/2011JB008916.
- 610 21. Pritchard, H. D., Ligtenberg, S. R. M., Fricker, H. A., Vaughan, D. G., Van den Broeke,
611 M. R., & Padman, L. (2012). Antarctic ice-sheet loss driven by basal melting of ice
612 shelves. *Nature*, 484(7395), 502-505.
- 613 22. Rignot, E., Mouginot, J. & Scheuchl, B. (2011), Ice flow of the Antarctic ice sheet.
614 *Science*, 333(6048), 1427-1430.
- 615 23. Rignot, E., & Jacobs, S. S. (2002). Rapid bottom melting widespread near Antarctic ice
616 sheet grounding lines. *Science*, 296(5575), 2020-2023.
- 617 24. Scambos, T. Hulbe, A., C. & Fahnestock, M. A. (2003). Climate-induced ice shelf
618 disintegration in the Antarctic Peninsula. *Antarctic Research Series*, 79, 79-92.
- 619 25. Scambos, T. Hulbe, A., C. Fahnestock, M. A. & Bohlander, J. (2000). The link between
620 climate warming and breakup of ice shelves in the Antarctic Peninsula. *Journal of*
621 *Glaciology*, 46(154), 516-530.
- 622 26. Shepherd, A., Wingham, D., Payne, T., & Skvarca, P. (2003). Larsen Ice Shelf has
623 progressively thinned. *Science*, 302(5646), 856-859.
- 624 27. Shuman, C. A., Zwally, H. J., Schutz, B. E., Brenner, A. C., DiMarzio, J. P., Suchdeo, V.
625 P., & Fricker, H. A. (2006). ICESat Antarctic elevation data: Preliminary precision and
626 accuracy assessment. *Geophysical Research Letters*, 33(7).

- 627 28. Smith, K. L., Robison, B. H., Helly, J. J., Kaufmann, R. S., Ruhl, H. A., Shaw, T. J., ... &
628 Vernet, M. (2007). Free-drifting icebergs: hot spots of chemical and biological
629 enrichment in the Weddell Sea. *Science*, 317(5837), 478-482.
- 630 29. Smith, K. L. (2011). Free-drifting icebergs in the Southern Ocean: an overview. *Deep Sea*
631 *Research Part II: Topical Studies in Oceanography*, 58(11), 1277-1284.
- 632 30. Tamura, T., Williams, G. D., Fraser, A. D. & Ohshima, K. I. (2012). Potential regime
633 shift in decreased sea ice production after the Mertz Glacier calving, *Nature*
634 *communications*, 3, 826.
- 635 31. Van den Broeke, M. (2008). Depth and density of the Antarctic firn layer. *Arctic,*
636 *Antarctic, and Alpine Research*, 40(2), 432-438.
- 637 32. Wang, X.W., Cheng, X., Gong, P., Huang, H. B., Li Z., & Li, X. W. (2011). Earth
638 Science Applications of ICESat/GLAS: a Review. *International Journal of Remote*
639 *Sensing*, 32, 23, 8837-8864, doi: 10.1080/01431161.2010.547533
- 640 33. Wang, X.W., Cheng, X., Gong, P., Shum, C. K., Holland, D.M., & Li, X.W. (2014).
641 Freeboard and mass extraction of the disintegrated Mertz Ice Tongue with remote sensing
642 and altimetry data. *Remote Sensing of Environment*, 144, 1-10.
- 643 34. Wang, X.W. (2014). Mertz ice tongue evolutions from satellite observed data,
644 Postdoctoral Research Report, College of Global Change and Earth System Science,
645 Beijing Normal University, China. doi: 10.13140/2.1.1006.1603
- 646 35. Wang, X., Cheng, X., Li, Z., Huang, H., Niu, Z., Li, X., & Gong, P. (2012). Lake water
647 footprint identification from time-series ICESat/GLAS data. *Geoscience and Remote*
648 *Sensing Letters, IEEE*, 9(3), 333-337.

- 649 36. Wang, X., Gong, P., Zhao, Y., Xu, Y., Cheng, X., Niu, Z., ... & Li, X. (2013). Water-
650 level changes in China's large lakes determined from ICESat/GLAS data. *Remote Sensing*
651 *of Environment*, 132, 131-144.
- 652 37. Yi, D., Zwally, H.J., & Robbins, J. (2011). ICESat observations of seasonal and
653 interannual variations of sea-ice freeboard and estimated thickness in the Weddell Sea,
654 Antarctica (2003-2009). *Annals of Glaciology*, 52(57), 43-51.
- 655 38. Zwally, H. J., Schutz, B., Abdalati, W., Abshire, J., Bentley, C., Brenner, A., Buftona, J.,
656 Deziouf, J., Hancocka, D., Hardinga, D., Herringg, T., Minsterh, B., Quinng, K., Palmi,
657 S., Spinhirnea, J., & Thomasj, R. (2002). ICESat's laser measurements of polar ice,
658 atmosphere, ocean, and land. *Journal of Geodynamics*, 34, 405-445.
- 659 39. Zwally, H. J., Yi, D., Kwok, R., & Zhao, Y. (2008). ICESat measurements of sea ice
660 freeboard and estimates of sea ice thickness in the Weddell Sea. *Journal of Geophysical*
661 *Research*, 113, C02S15, doi:10.1029/2007JC004284.
- 662

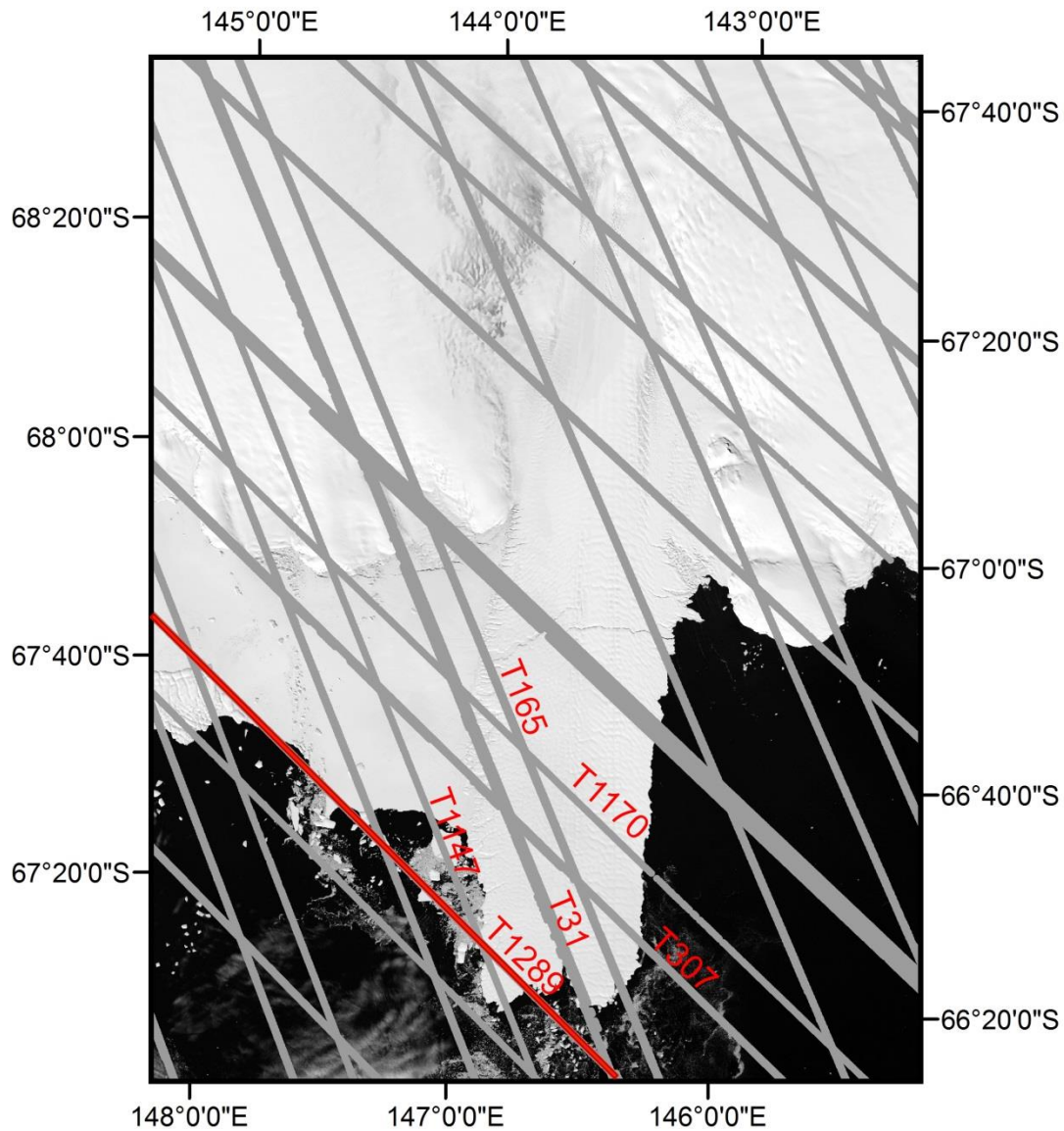
Figures



664

665 **Figure 1.** Mertz Ice Tongue (MIT), East Antarctica. Landfast sea ice is attached to the east flank
 666 of the MIT and the Mertz Polynya is to the west. The background image is from band 4 Landsat
 667 7, captured on February 2, 2003. The green square found in the upper left inset indicates the
 668 location of the MIT in East Antarctica. A polar stereographic projection with -71 °S as standard
 669 latitude is used.

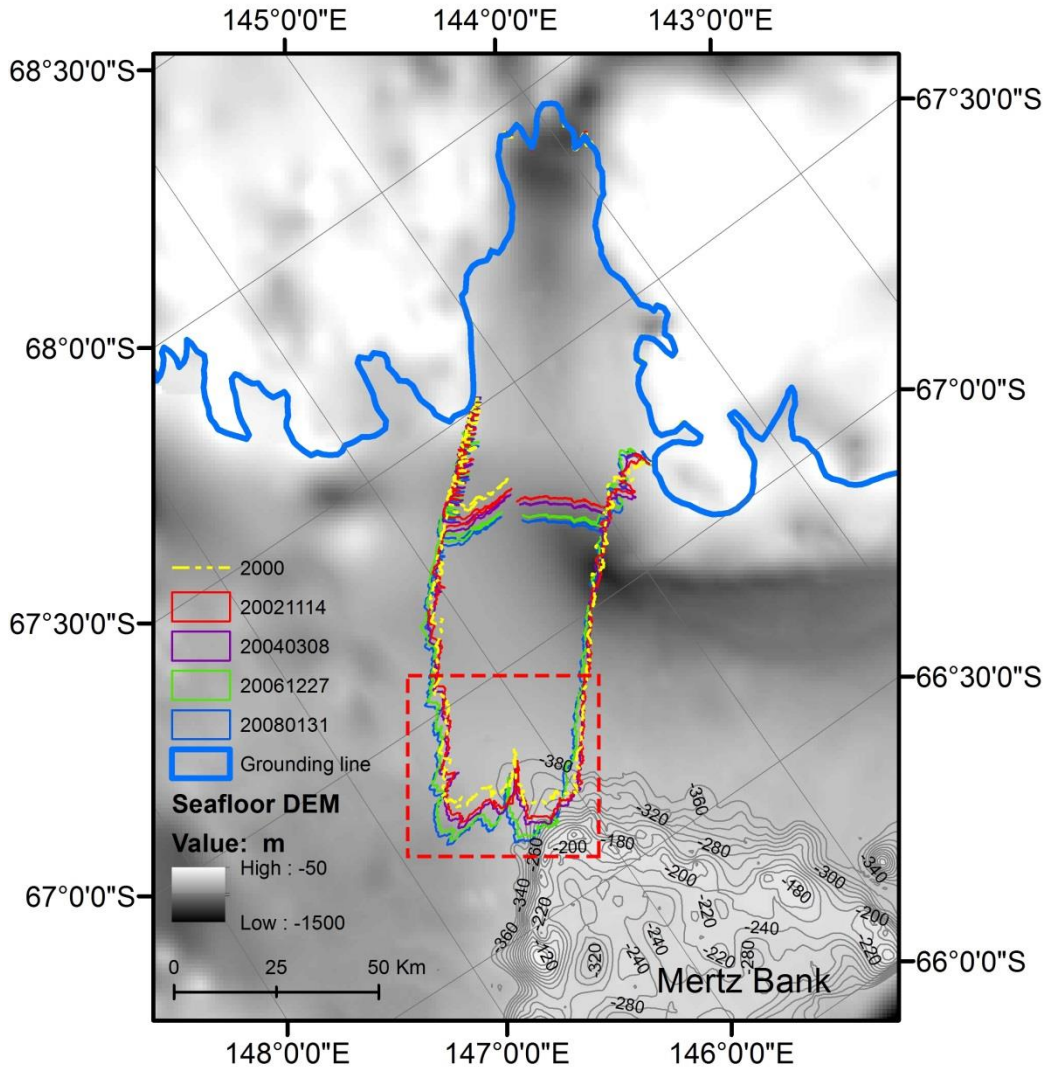
670



671

672 **Figure 2.** Spatial distribution of ICESat/GLAS data from 2003 to 2009 covering the Mertz
673 region. Ground tracks of ICESat/GLAS are indicated with gray lines. Track 1289 (T1289) is
674 highlighted in red as is used in Fig. 4. The background image is from band 4 Landsat 7, captured
675 on February 2, 2003. A polar stereographic projection with -71 °S as standard latitude is used.

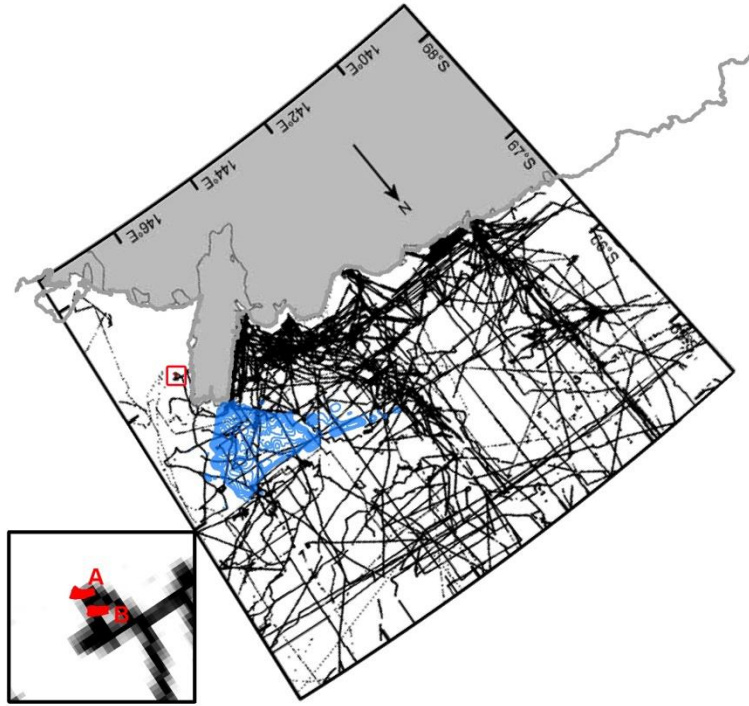
676



677

678

(a)



679

680

(b)



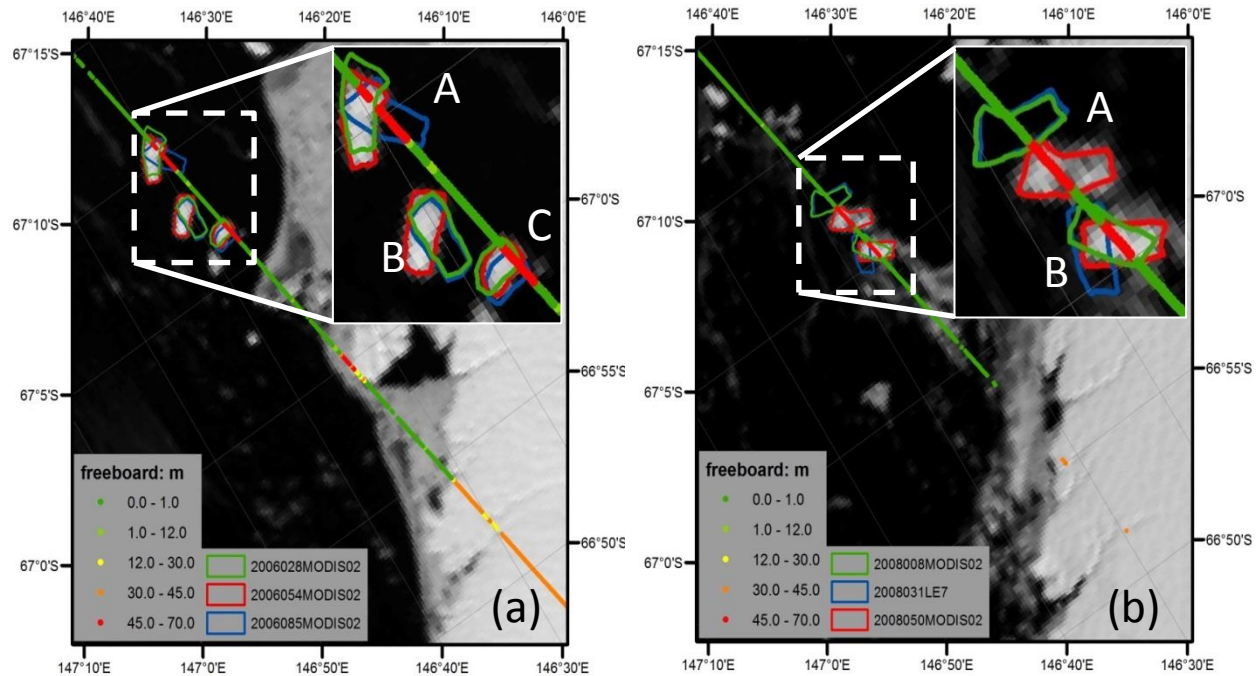
681

682

683

(c)

684 **Figure 3.** (a) Seafloor topography from bathymetry around Mertz region and outlines of the
685 MIT from 2002 to 2008. The outlines of the MIT in different years are marked with different
686 colored polygons. The shallow Mertz Bank is located in the lower right (northeast). The yellow
687 dash-dotted line indicates the shape of the MIT on January 25, 2000, which is used to identify
688 the bathymetry gap under the ice tongue. The dashed red inset box corresponds to location of
689 Figs. 6 and 7. (b) : multi-beam bathymetry dataset coverage over the Mertz region. The
690 embedded figure in the lower left is the zoom in of the red rectangle which shows the positions
691 of iceberg ‘A’ and ‘B’ (polygon filled in red) on February 19, 2008 (Fig. 4). (c): single-beam
692 bathymetry dataset coverage over the Mertz region. Blue polylines show the contours around the
693 Mertz Bank and black dots are measurement profiles. (b) and (c) are redrawn from Beaman et al.
694 (2011) because original spatial coverage of the single and multi-beam bathymetry data is not
695 available. However, for being able to use the Figures from Beaman et al. (2011), we geo-
696 registered it and put the contour around Mertz Bank and location of icebergs used in the text over
697 it, from which the density of bathymetry measurement can be clear. From the coastline from
698 Radarsat Antarctic Mapping Project-2000 indicated with the thick gray line in (b) and (c), we can
699 conclude that the geo-registration is successful as it coincides with that from Beaman et al. (2011)
700 well in most parts. This Figure is under a projection of polar stereographic projection with -71 °S
701 as standard latitude.

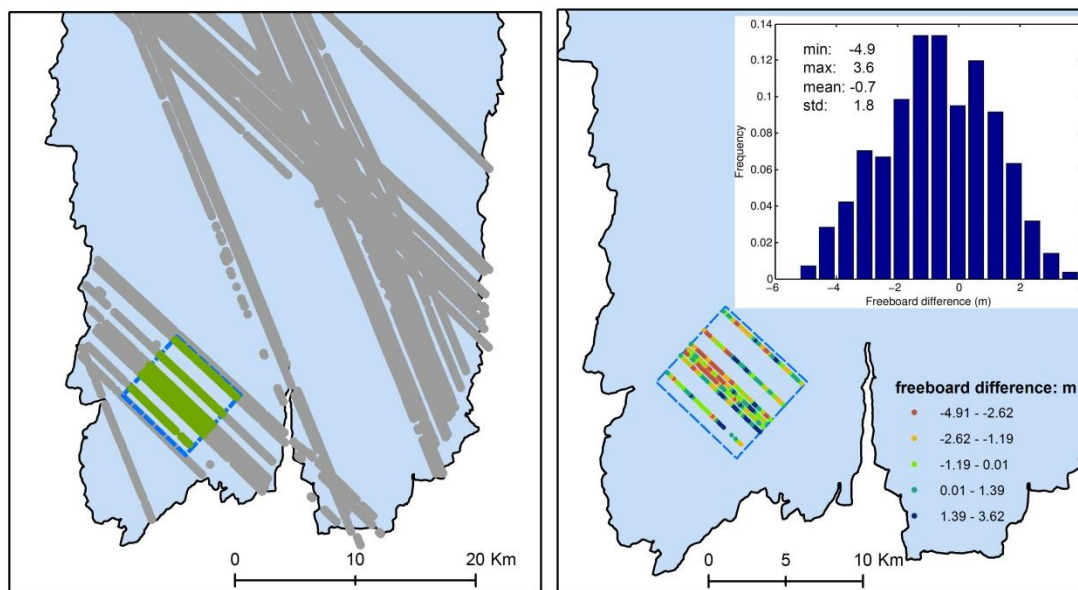


702

703 **Figure 4.** Freeboard extracted from Track 1289, ICESat/GLAS, the location of which can be
 704 found in Fig. 2 and Fig. 3(b). (a) and (b) show the freeboard extracted from ICESat/GLAS on
 705 February 23, 2006 (2006054) and February 18, 2008 (2008049) respectively. In each image,
 706 positions of three icebergs (with name labeled as ‘A’, ‘B’ and ‘C’) closest to ICESat/GLAS
 707 observation time are plotted with green, red and blue polygons respectively. The dates are
 708 indicated with seven numbers (yyyyddd) in legend. ‘yyyyddd’ stands for day ‘ddd’ in year
 709 ‘yyyy’. ‘MODIS02’ and ‘LE7’ indicate that the image used to extract iceberg outline is from
 710 MODIS and Landsat 7 ETM+, respectively.

711

712



713

714

(a)

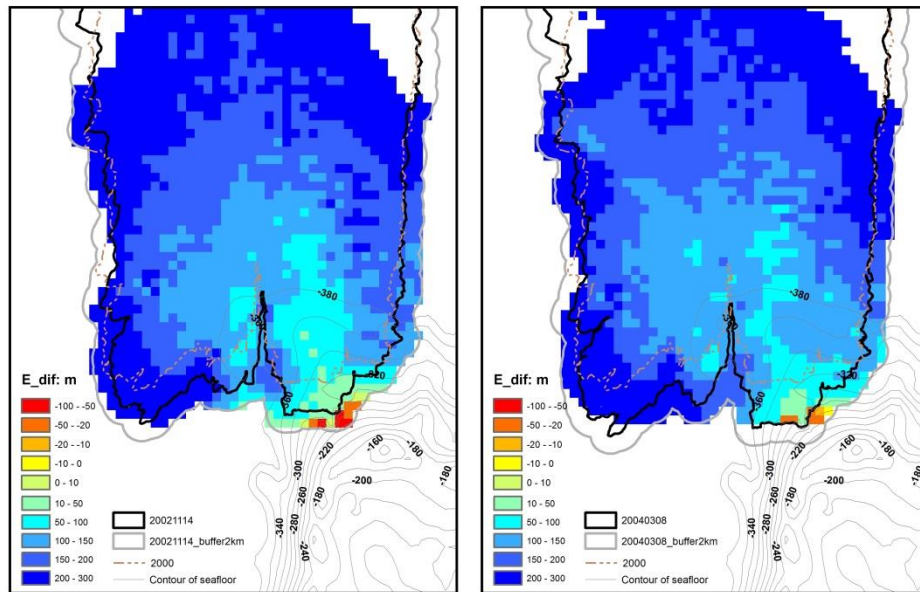
(b)

715 **Figure 5.** Evaluation of kriging interpolation method over the MIT using freeboard data derived
716 from ICESat/GLAS. (a) shows profile locations of freeboard derived from ICESat/GLAS after
717 relocation over the MIT. Gray dots indicate ICESat/GLAS used for interpolation using kriging
718 method. The blue dashed square indicates the region used to investigate interpolation accuracy of
719 kriging method, about 7 km \times 7 km. Inside of the square, freeboard data marked with green dots
720 are used to check the accuracy of freeboard interpolated with kriging. (b) is the freeboard
721 comparison result derived by subtracting krigged freeboard from freeboard derived from
722 ICESat/GLAS. The spatial distribution and the histogram of freeboard difference are shown in
723 the lower left and upper right respectively. The black polygon filled with light blue shows the
724 boundary of MIT on November 14, 2002.

725

726

727

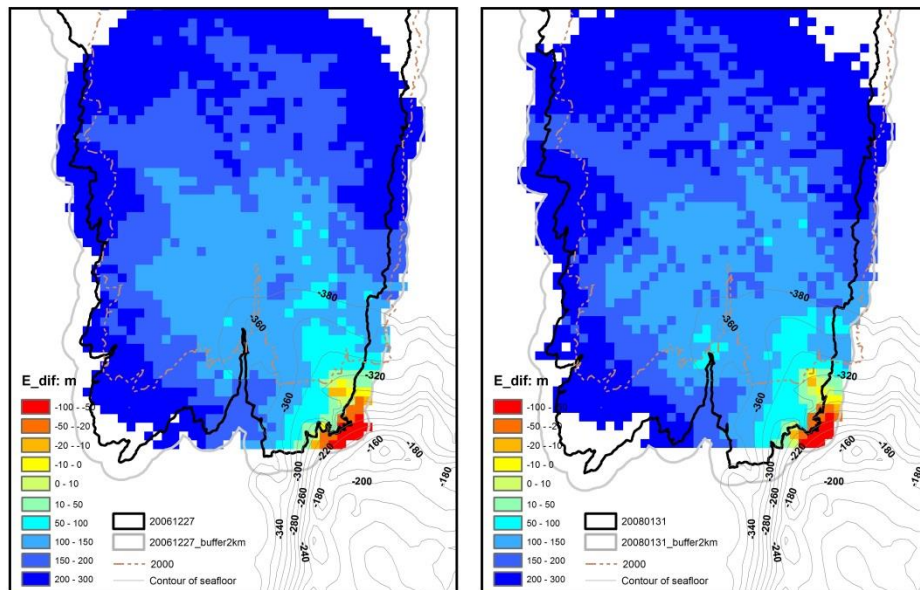


728

729

(a)

(b)



730

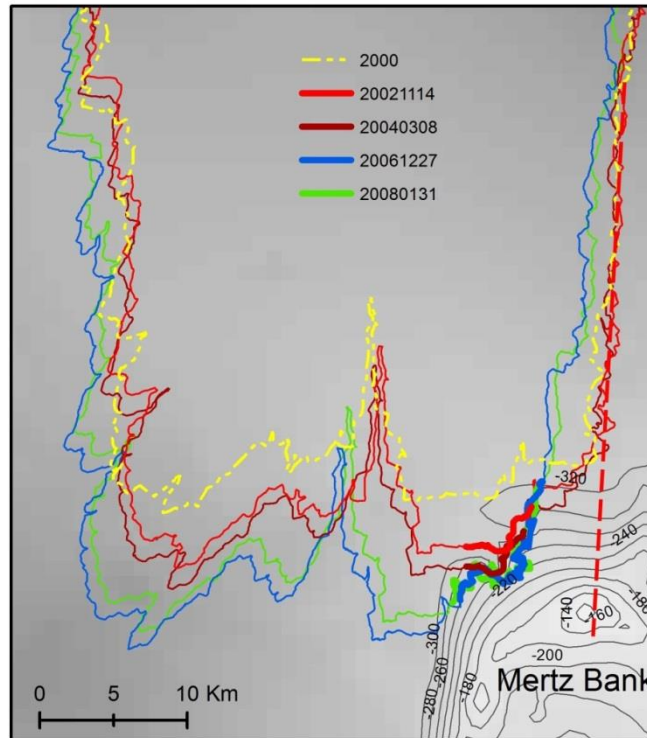
731

(c)

(d)

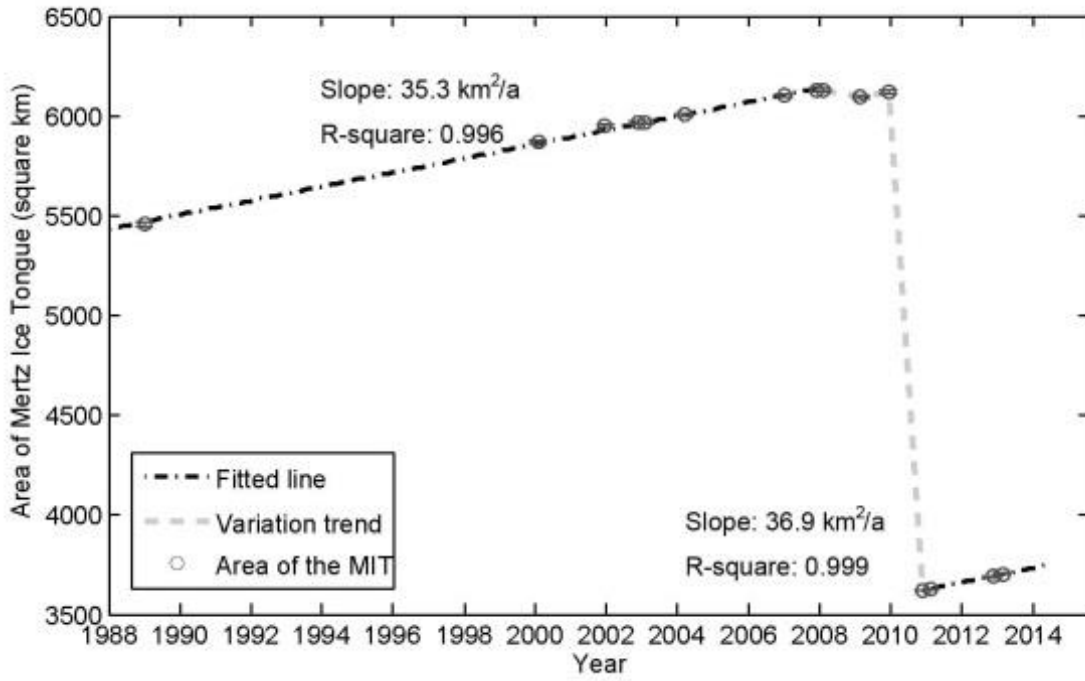
732 **Figure 6.** Elevation difference of Mertz ice bottom and seafloor topography. (a), (b), (c) and (d)
733 correspond to elevation difference assuming hydrostatic equilibrium under the minimum sea
734 surface height -3.35 m on November 14, 2002 , March 8, 2004, December 27, 2006, and January

735 31, 2008, respectively. The contours in the lower right indicate seafloor topography (unit: m) of
736 the Mertz Bank with an interval of 20 m. The solid black line indicates the boundary of the MIT
737 and the thick gray line outlines a buffer region of the boundary with 2 km as buffer radius. The
738 dash-dotted line indicates the shape of the MIT on January 25, 2000, which is used to identify
739 the bathymetry gap under the ice tongue. In the legend, negative values mean that ice bottom is
740 lower than the seafloor, which of course is impossible. Therefore, the initial assumption of a
741 floating ice tongue was incorrect in those locations (yellow to red colors), and the ice was
742 grounded. Regions with more negative values indicate more heavily grounding inside of the MIT
743 or more heavily grounding potential in the buffer region.



744

745 **Figure 7.** Digital Elevation Map (DEM) of seafloor around Mertz and grounding section of the
 746 boundaries extracted from 2002 to 2008. The grounding sections of the MIT boundary in 2002,
 747 2004, 2006 and 2008 is marked with thick red, purple, green and blue polylines respectively and
 748 MIT boundaries are indicated with polygons with the same legend as Fig. 3a. Additionally, MIT
 749 boundary in 2000 indicated with dash-dotted yellow polygon is used to show the different quality
 750 of seafloor DEM. Inside of this polygon no bathymetry data was collected or used. The dashed
 751 red line indicates the ‘extension line’ of the west flank of MIT on November 14, 2002, passing
 752 the shallowest region of the Mertz Bank (about -140 m).



753

754 **Figure 8.** Time series of area change of the MIT. The area covers the entire ice tongue, to the
 755 grounding line as indicated with thick blue line in Fig. 3a. The area is extracted from Landsat
 756 images from 1988 to 2013.

757

Tables

758 **Table 1.** Statistics of the icebergs used to inverse FAC with least-square method and validation
 759 of grounding iceberg detection using this FAC. Icebergs ‘A’, ‘B’ and ‘C’ are the same as what
 760 are used in Fig. 4 and S-Fig 1. Measurements from icebergs ‘A’ and ‘C’ in February 2006 are
 761 used to derive FAC with least-squares method. Icebergs ‘A’ and ‘B’ in 2008 are used for
 762 validation.

Icebergs	date	Latitude	Longitude	Freeboard	Seafloor	Sea Surface Height	ε	E_{dif}
		($^{\circ}$)	($^{\circ}$)	(m)	(m)	(m)	(m)	(m)
A	Feb 23, 2006	-67.1737	146.6595	66.88	-528.48	-1.92	0.89	
		-67.1752	146.6604	66.34	-527.01	-1.92	1.30	
C	Feb 23, 2006	-67.1085	146.6247	66.37	-505.84	-1.92	-	1.25
		-67.1100	146.6255	66.28	-507.08	-1.92	-	1.01
A	Feb 18, 2008	-67.1194	146.6303	58.88	-522.52	-2.08		69.14
		-67.1209	146.6311	59.58	-524.16	-2.08		64.88
B	Feb 18, 2008	-67.0906	146.6151	67.22	-500.92	-2.08		-
		-67.0921	146.6159	66.10	-500.47	-2.08		22.45
								-
								13.55

763

764 **Table 2.** Statistics of grounding grids inside or grounding potentials outside of the Mertz Ice
765 Tongue (MIT) ('I': inside of thick black line, Fig. 6; Number in brackets indicates how many
766 grids are located inside of the 2000 Mertz boundary; 'O': between the black and gray lines, Fig.
767 6) on November 14, 2002, March 8, 2004, December 27, 2006 and January 31, 2008 respectively.
768 Each grid covers an area of 1 km². The Mean, Minimum and Standard deviation is calculated
769 without considering those fallen inside of the 2000 Mertz boundary, but only those having
770 elevation difference less than 46 m and out of 2000 Mertz boundary.

771

Elevation difference (subtracting seafloor from ice bottom)	2002-11-14		2004-03-08		2006-12-27		2008-01-31	
	I	O	I	O	I	O	I	O
23-46 (m)	9(3)	10(0)	6(0)	3(0)	10(1)	1(0)	10(3)	5(0)
0-23 (m)	2(0)	6(0)	1(0)	1(0)	9(0)	2(0)	4(0)	2(0)
<0 (m)	0(0)	8(0)	2(0)	5(0)	7(0)	21(0)	6(0)	18(0)
Mean (m)	28.8	9.8	15.8	-1.1	10.9	-41.9	12.3	-31.0
Minimum (m)	11.9	-81.5	-46.0	-44.5	-52.3	-102.8	-34.8	-103.0
Standard deviation (m)	9.2	36.8	29.6	31.4	24.7	37.6	27.3	38.0
Number of grids	8	24	9	9	25	24	17	25

772

773 **Table 3.** Statistics of grounding outlines of the MIT as shown with thick polylines in Fig. 7 on
 774 November 14, 2002, March 8, 2004, December 27, 2006 and January 31, 2008 respectively

	2002-11-14	2004-03-08	2006-12-27	2008-01-31
Start location (°)	146.124 °E, 66.696 °S	146.155 °E, 66.681 °S	146.093 °E, 66.700 °S	146.088 °E, 66.699 °S
End location (°)	146.240 °E, 66.693 °S	146.256 °E, 66.683 °S	146.304 °E, 66.669 °S	146.292 °E, 66.668 °S
Perimeter (km)	7.0	6.4	24.7	20.9

775